Acta Geotechnica (2023) 18:6759–6773
https://doi.org/10.1007/s11440-023-01875-8

RESEARCH PAPER

Quantitative bearing capacity assessment of strip footings adjacent to two-layered slopes considering spatial soil variability

Haizuo Zhou[1,2,3] · Qichao Hu[1,2] · Xiaoxuan Yu[1,2] · Gang Zheng[1,2,3] · Xiangning Liu[1,2] · Huajun Xu[4] · Shangchuan Yang[5,6] · Jun Liu[7] · Kan Tian[7]

Received: 15 August 2022 / Accepted: 8 March 2023 / Published online: 14 April 2023

Abstract

The probabilistic bearing capacity of the strip footing placed near a two-layered cohesive soil slope is evaluated using random adaptive finite element limit analysis with anisotropic random field modeling and Monte Carlo simulation techniques. To account for the combined effect of geometric parameters (i.e., normalized slope heights, and slope angles), soil properties (i.e., ratio of undrained shear strength from two-layer soils) and spatially variable strengths of two-layered soil, the bearing capacity is quantitatively examined in stochastic analysis. Moreover, a sensitivity analysis is exhibited, and the optimal layout of footings near a two-layered slope is estimated through a multivariate adaptive regression splines procedure. The associated results demonstrate that the slope angle has the most significant impact on the mean bearing capacity, while the coefficient of variation of the ultimate bearing capacity factor could be greatly reduced by decreasing the variability of the upper layer soil. The interaction effects between these influencing factors are numerically investigated. This study highlights the prominent role of the variability in lower layer soil when the coupled influence of geometric conditions and soil properties is considered.

Keywords Bearing capacity · Finite element limit analysis · Random fields · Slope stability · Spatial variability · Two-layered soil slope

List of symbols

$N_{c,det}$	Bearing capacity factor under deterministic analysis
q_u	Average limit pressure under the footing
c_{u1}	Undrained shear strength of upper layer
c_{u2}	Undrained shear strength of lower layer
$c_{u1}/\gamma B$	Normalized shear strength of upper layer
$c_{u2}/\gamma B$	Normalized shear strength of lower layer
c_{u1}/c_{u2}	Undrained shear stress ratio
γ	Self-weight of soils
B	Footing width
H	Slope height
λ	Normalized footing distance
β	Slope angle
H/B	Normalized slope height
D/B	Normalized thickness of the top layer
N_{su}	Normalized undrained shear strength
N_c	Bearing capacity factor
i	The counter for the random field realization
$q_{u,\ i}$	Ultimate bearing capacity of the footing
θ_x	Horizontal correlation length
θ_y	Vertical correlation length
μ_{Nc}	Mean bearing capacity factor
COV	Coefficient of variation
COV_{Nc}	Coefficient of variation of the bearing capacity factor

✉ Xiaoxuan Yu
yuxiaoxuan@tju.edu.cn

[1] School of Civil Engineering, Tianjin University, Tianjin 300072, China

[2] Key Laboratory of Coast Civil Structure Safety, Ministry of Education, Tianjin University, Tianjin 300072, China

[3] State Key Laboratory of Hydraulic Engineering Simulation and Safety, Tianjin University, Tianjin 300072, China

[4] Anhui Transport Consulting & Design Institute Co, Ltd, Hefei 230088, China

[5] School of Civil Engineering, Southwest Jiaotong University, Chengdu 610031, China

[6] Key Laboratory of High-Speed Railway Engineering of the Ministry of Education, Southwest Jiaotong University, Chengdu 610031, China

[7] College of Urban-Rural Planning and Civil Engineering, Guiyang University, Guiyang 550005, China

COV_{cu1} Coefficient of variation of upper layer
COV_{cu2} Coefficient of variation of lower layer

1 Introduction

Due to stringent limitations of the ground in practice, buildings are often constructed on or near native or engineered slopes [1, 7]. Investigations focused on the presence of slopes can ineluctably have an adverse effect on the ultimate bearing capacity of strip footings. Analytical solutions have been reported by Kusakabe et al. [19], Leshchinsky and Ambauen [20], Meyerhof [28] and Yang et al. [44] to estimate the ultimate bearing capacity of foundations placed atop slopes. Associated with bearing capacity, the corresponding failure mechanism was also observed by Georgiadis [7] based on finite element (FE) analyses. Leshchinsky [21] investigated the bearing capacity and the associated failure mechanism of a strip footing resting on a slope considering the influence of the slope angle, footing width and soil strength properties. Zhou et al. [55, 56] quantitatively defined the threshold between the bearing capacity and slope stability issues and presented detailed design charts under static and seismic conditions. In reality, natural soils are often deposited in layers [10]. Recently, more attention has been drawn to the bearing capacity of foundations placed on the top of two-layered soil slopes. Investigations have been conducted to estimate the ultimate bearing capacity of a layered soil by experiments and numerical modeling [2–4, 6, 13–15, 23, 29, 30, 34, 40, 53, 57]. Merifield et al. [30] investigated the bearing capacity of a rigid footing on horizontal ground composed of two-layered clay. Wu et al. [39] and Xiao et al. [41] conducted a series of parametric studies to investigate the interaction effects of geometrical parameters and soil properties on the ultimate bearing capacity and failure mechanism for footings adjacent to two-layered soil slopes.

Prior works have offered significant guidance to evaluate the ultimate bearing capacity of strip footings resting on two-layered slopes under different situations through deterministic analysis. However, it has been confirmed, in a large proportion of engineering cases, that soil properties such as the shear strength parameters are uncertain with spatial variations [31, 37, 58]. The bearing capacity of rigid footings resting on the top of single-layered slopes considering the spatial variability of soils has received attention. Luo and Bathurst [27] investigated the influence of single-layered soil parameters and geometric conditions on the mean bearing capacity and its variability considering the spatial variability of purely cohesive soils. Halder and Chakraborty [11, 12] quantified the variation trends of bearing capacity in spatially variable soils with various slope angles. They quantified the bearing capacity reduction for footings constructed on the top of a single-layered slope. However, prior assessments of bearing capacity do not involve two-layered soil slopes. Meanwhile, few studies have revealed how the spatial variability of random soil quantitatively affects the interaction of influential factors.

The objective of this paper is to investigate the coupled effect of the spatial variability of undrained shear strength on the ultimate bearing capacity of a rigid footing on a two-layered soil slope with idealized geometry. The analyses are carried out by using a random adaptive finite element limit analysis (RAFELA) [18]. Influential factors, including geometric conditions (e.g., normalized slope height, slope angle), soil parameters (e.g., undrained shear strength) and the soil spatial correlation parameters (i.e., the coefficients of variation (COVs) and the ratio of vertical and horizontal correlation lengths (θ_y/θ_x) for two-layered soils), are analyzed to reveal the relationship between the ultimate bearing capacity and the coupled influence of soil parameters. Finally, the sensitivity of the affecting parameters as well as their interaction effects are discussed by adopting a multivariate adaptive regression splines (MARS) procedure.

2 Problem definition and validation

A general layout of the model is illustrated in Fig. 1. A rigid rough footing of width B is positioned adjacent to a two-layered soil slope with height H and angle β. The top layer of clay with undrained shear strength c_{u1} is underlain by a clay layer with c_{u2}. The value of slope height is equal to that of the thickness of the top layer. The ultimate bearing capacity q_u for a rigid footing can be described as [30]:

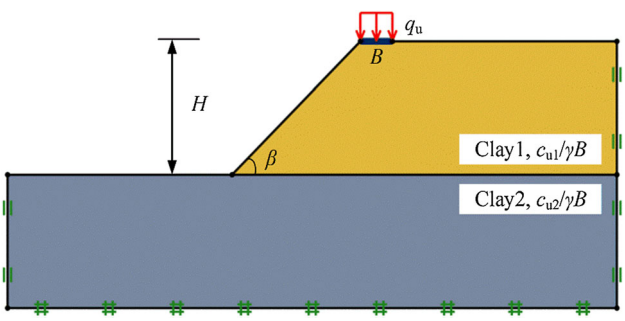

Fig. 1 Schematic of the model

$$q_u = c_{u1} \times N_c = f\left(\frac{H}{B}, \beta, \frac{c_{u1}}{c_{u2}}\right) \quad (1)$$

where q_u = average limit pressure under the footing; c_{u1} = undrained shear strength of the upper layer; c_{u2} = undrained shear strength of the lower layer; B = footing width; H = slope height; and β = slope angle. The interface between the rigid footing and the soil is assumed to be rough in this study [14]. The bottom and side boundaries are fixed in both the horizontal and vertical directions, whereas vertical displacement is allowed for the side boundaries. To ensure negligible boundary effects, the boundaries are placed far enough away from the footing.

Owing to acting as a rigorous analytical solution, Finite Element Limit Analysis (FELA) combines the finite element method (FEM) with the limit analysis theory to calculate the collapse load of a structure. To investigate the bearing capacity of footings on horizontal ground [36, 51] and footings on slopes [7, 21, 56], an upper-bound (UB) LA has commonly been employed in prior investigations. The assumption with perfectly plastic soils is proposed, in which an associated flow rule is obeyed for the upper-bound theorem of plasticity. With reference to the rule, the power dissipated for a kinematically admissible velocity field equals that dissipated by external loading, which enables determination of an upper bound for the ultimate bearing capacity and failure geometry [36]. In this study, numerical analyses are carried out with UBLA, and the method is rigorously based on plasticity theorems and has been successfully used in prior investigations [1, 16, 17, 22, 39, 42, 45, 51].

To verify the accuracy of the established model, the bearing capacity of a footing on two-layered cohesive soil slopes (N_c) predicted in this study is compared with the results presented in prior investigations. A series of comparisons between the proposed method and the undrained solutions of Xiao et al. [41], Kalourazi et al. [15] and Izadi et al. [14] are shown in Fig. 2, and the corresponding parameters are shown in Table 1. An agreement in terms of N_c or $N_{\gamma s}/N_{\gamma LG}$ is found between the calculated results and prior investigations for footings adjacent to two-layered slopes, as shown in Fig. 2.

3 RAFELA modeling

The undrained shear strength of two-layer soils is considered with anisotropic spatial variability for probabilistic investigations of the bearing capacity of footing on slopes. Following previous studies [8, 9, 23–26, 31], it is assumed that the undrained shear strength in this study obeys a lognormal distribution and can be expressed as follows:

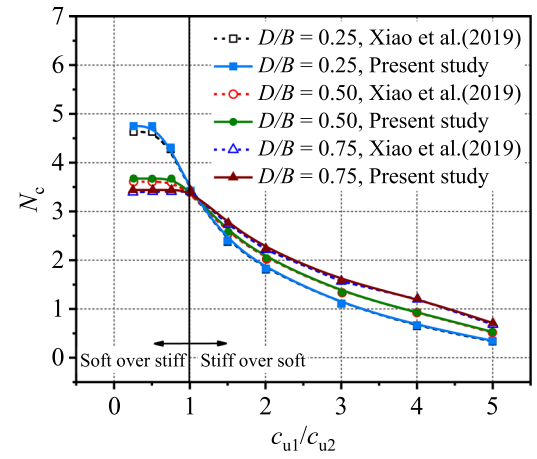

(a)

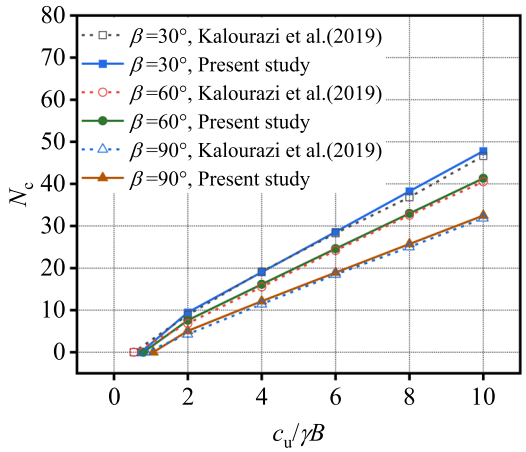

(b)

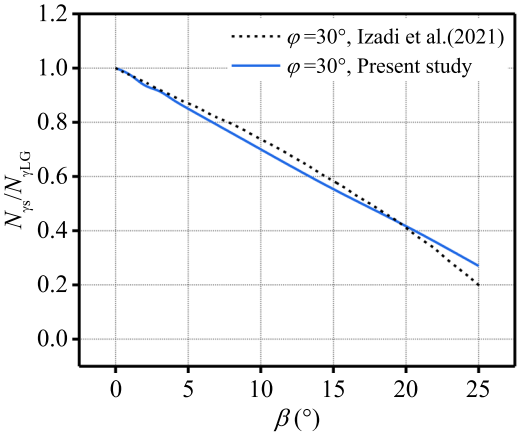

(c)

Fig. 2 Comparison of bearing capacity with the results from prior investigations: **a** Xiao et al. [41]; **b** Kalourazi et al.[15]; **c** Izadi et al. [14]

Table 1 Parameters of ultimate bearing capacity analysis of a rigid footing on a two-layered soil slope for calibration [14, 15, 41]

Parameter	Value [41]	Value [15]	Value [14]
Normalized shear strength of top layer, $c_{u1}/\gamma B$	1, 2, 4, 6, 8, 10	0.5–1, 2, 4, 6, 8, 10	/
Undrained shear stress ratio, c_{u1}/c_{u2}	0.25–5	1	/
Internal friction angle, φ(°)	0	0	30
Slope height to footing width ratio, H/B	0.5–3	4	4
Slope angle, β (°)	15, 30, 45	30, 60, 90	0–25
Footing width, B (m)	1	1	1
Self-weight of soils, γ (kN/m^3)	20	20	20
Normalized footing distance λ (i.e., footing distance/footing width)	0–2.5	1	0
Normalized thickness of the top layer, D/B	0.25–1.5	4	4

$$f(x) = \frac{1}{x\sigma_{\ln x}\sqrt{2\pi}}\exp\left[-\frac{1}{2}\left(\frac{\ln x - \mu_{\ln x}}{\sigma_{\ln x}^2}\right)^2\right] \tag{2}$$

where the mean $\mu_{\ln x}$ and standard deviation $\sigma_{\ln x}$ meet:

$$\mu_{\ln x} = \exp\left(\mu_{\ln x} + \frac{\sigma_{\ln x}^2}{2}\right) \tag{3}$$

$$\sigma_{\ln x} = \sqrt{\exp\left(2\mu_{\ln x} + \sigma_{\ln x}^2\right)\left[\exp\left(\sigma_{\ln x}^2\right) - 1\right]} \tag{4}$$

The mean and standard deviation of undrained shear strength can be described in terms of COV, a dimensionless coefficient that depicts the inherent variability of undrained shear strength in a random field. It can facilitate designers to develop an appreciation for the probable range of variability inherent in the overall evaluation of common design soil properties and therefore identify atypical geotechnical variabilities [8, 31]:

$$\mathrm{COV} = \frac{\sigma_{\ln x}}{\mu_{\ln x}} \tag{5}$$

In a random field, soil properties spatially vary, and the correlation in space is considered. To incorporate the spatial variability of soil, the Karhunen–Loeve (KL) expansion is adopted by identifying a set of orthogonal basis functions that can capture the variability of the field using a small number of terms. The spatial correlation structure is represented by a parameter called "correlation length (θ)" [8, 31], which is a measure of the distance within which the properties are noticeably correlated. A larger θ implies that the fluctuation of the soil property is spatially slower and the soil is more homogeneous, whereas a smaller θ implies that the soil property fluctuates more rapidly in the space and the soil is more homogeneous. To describe the fluctuation of anisotropic random fields, two important terms, the horizontal and vertical correlation lengths (θ_x and θ_y, respectively), are introduced. In the context of K-L expansion, a 2D normally distributed random field $H(x, y)$ can be discretized based on the spectral decomposition of its cocorrelation function $p[(x_1, y_1), (x_2, y_2)]$. This field is generally expressed as a truncated series as

$$H(x,y) = \hat{H}(x,y,\theta') = \mu' + \sum_{j=1}^{M}\sigma'\sqrt{\lambda_j}f_j(x,y)x_j(\theta') \tag{6}$$

where $\hat{H}(x, y, \theta')$ represents the simulated random field of $H(x, y)$, θ' denotes the coordinate in the decomposited outcome space; u' and σ' represent the mean and standard deviation of the random field, respectively; $f_j(x, y)$ and λ_j denote the eigenfunctions and eigenvalues of the correlation function $p[(x_1, y_1), (x_2, y_2)]$ obtained by solving the homogeneous Fredholm integral equation of the second kind [32, 33]; $x_j(\theta)$ is a set of uncorrelated random variables with zero mean and unit variance, and M represents the number of K–L expansion terms.

Phoon and Kulhawy [31] comprehensively investigated the effect of the correlation length and summarized a potential range of correlation lengths. To verify an accurate calculation, a sensitivity analysis is performed with adequate Monte Carlo simulations adopted in the discretization, as shown in Fig. 3. Therefore, a total of 1000 Monte Carlo simulations were adopted in each analysis.

4 Parametric analysis

4.1 Analysis of deterministic variables

To investigate the bearing capacity of a rigid footing on the top of cohesive soil slopes, a parametric study with a uniform soil domain is presented, covering four geometric parameters, namely, the normalized undrained shear

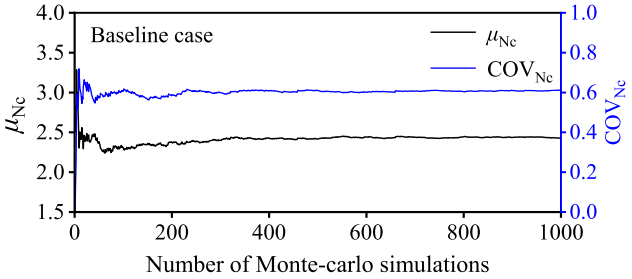

Fig. 3 Effect of the number of realizations on the bearing capacity factor statistics (baseline case): mean bearing capacity factor and variation in the COV of the bearing capacity factor

strength N_{su}, normalized slope height H/B, slope angle β and normalized footing distance from the crest of the slope λ (footing offset distance/footing width). The UB bearing capacity design chart curves for deterministic analyses are presented in Fig. 4. Three failure mechanisms are observed, including face failure, toe failure and overall slope failure [55]. For the face failure mode and toe failure, failure slips extend to the slope face and toe, respectively, and uniform soils are observed where an asymmetrical rigid wedge occurs directly beneath the footing. However, the slope failure mode, without showing distinct active and passive wedges, is attributed to the slope stability mechanism rather than the bearing capacity issue. The corresponding failure modes are depicted with design chart curves, in which cases serve as the baseline case (i.e., red dots) for the numerical results that appear later in the paper.

Table 2 Soil parameters used in the present study

Parameter	Value	Coefficient of variation
Normalized shear strength of top layer, $c_{u1}/\gamma B$	2	0.1–0.5
Normalized shear strength of bottom layer, $c_{u2}/\gamma B$	1, 2, 3, 4	0.1–0.5
Normalized slope heights, H/B	3, 4, 5	–
Slope angle, β	1:2, 1:1, 2:1	–
Self-weight of soils, γ (kN/m^3)	20	–
Horizontal spatial correlation length, θ_x (m)	10	–
Vertical spatial correlation length, θ_y (m)	1, 1.5, 2, 2.5	–
Normalized footing distance, λ	0	–

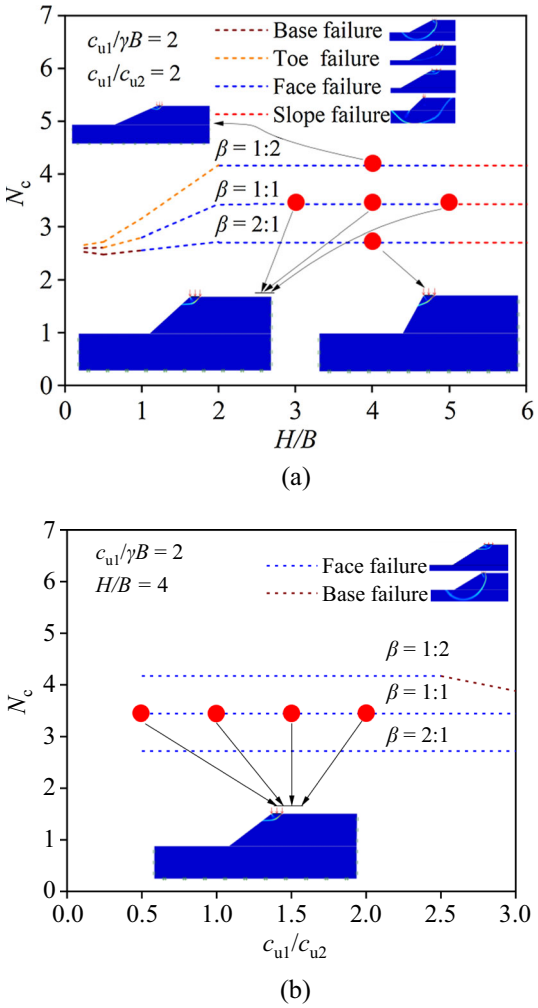

Fig. 4 Deterministic failure modes of different cases changing with **a** H/B and **b** c_{u1}/c_{u2} (the red dots represent the cases used in this study)

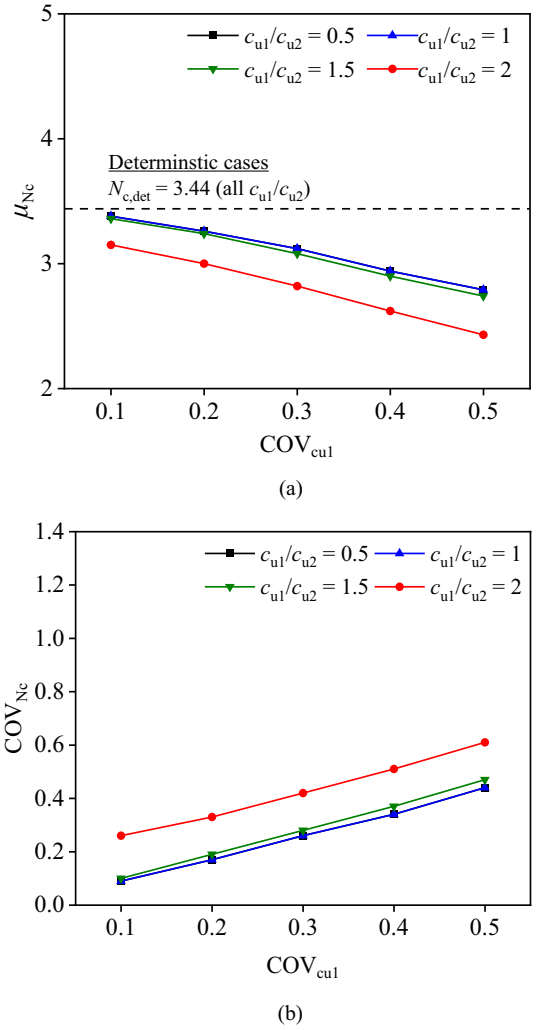

Fig. 5 Variation of mean and COV of bearing capacity factor (μ_{Nc} and COV_{Nc}, respectively) with COV of undrained shear strength of upper layer soil COV_{cu1} for different c_{u1}/c_{u2} ($c_{u1}/c_{u2} = 2$ is the baseline case): **a** mean of N_c; **b** COV of N_c

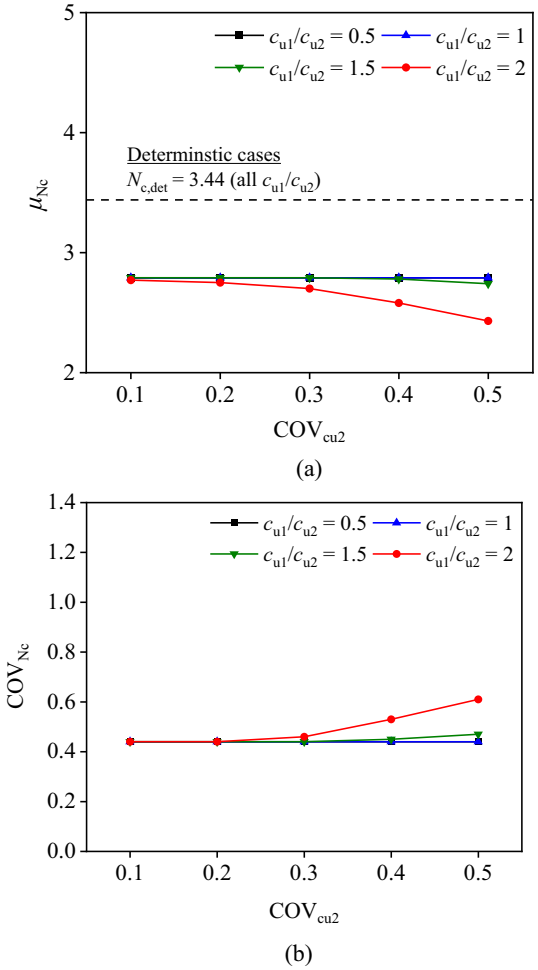

Fig. 6 Variation of μ_{Nc} and COV_{Nc} with COV of undrained shear strength of lower layer soil COV_{cu2} for different c_{u1}/c_{u2} (c_{u1}/c_{u2} = 2 is the baseline case): **a** mean of N_c; **b** COV of N_c

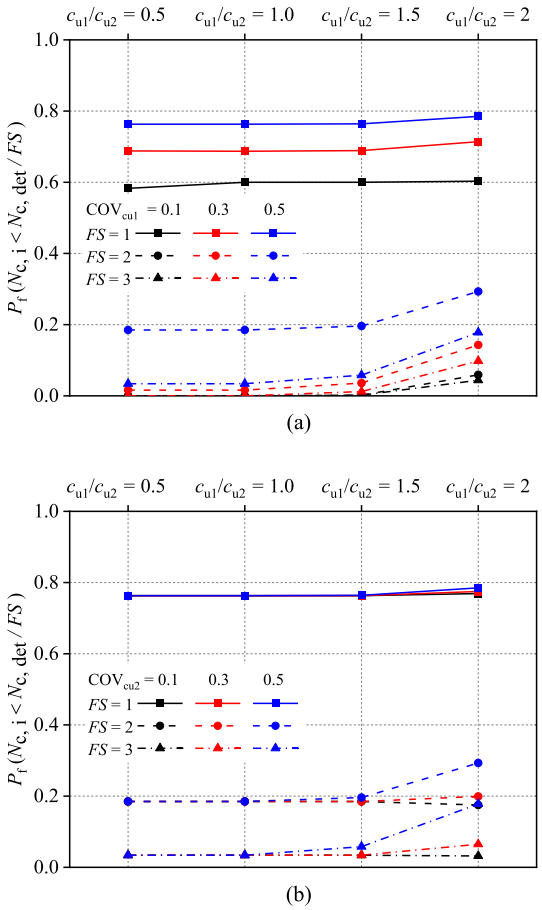

Fig. 7 Relationship between $P_f = P(N_{c,i} < N_{c,det}/FS)$ and c_{u1}/c_{u2} with various FS considering **a** COV_{cu1} and **b** COV_{cu2}

4.2 Stochastic analysis

To investigate the influence of affecting parameters on the bearing capacity, a certain parameter is changed from the baseline case (as shown in Table 2), while all other parameters are held constant. Equation 7 is used to calculate the bearing capacity factor N_c for each random field (i.e., each Monte Carlo simulation) as follows [27, 43]

$$N_{c,i} = q_{u,i}/\mu_c \tag{7}$$

where $q_{u,i}$ is the ultimate bearing capacity of the rigid footing and i is the counter for the random field realization. The q_u value is taken as 0 when slope failure occurs.

The ratio of the vertical and horizontal correlation distances θ_y/θ_x is maintained to represent the anisotropic property of the random field with various coefficients of variation of the soil cohesion COV_{Nc}. The COVs of the cohesion in the two layers vary from 0.1 to 0.5, and θ_y/θ_x ranges from 0.1 to 0.25 [27, 31]. In this study, the ratio of shear strength from the upper layer and lower layer clay c_{u1}/c_{u2} varies from 0.5 to 2, which covers most cases in practice [30]. Note that the ratio c_{u1}/c_{u2} is less than 1, corresponding to the case of a soft clay layer resting over a stiff clay layer, whereas c_{u1}/c_{u2} is greater than 1 corresponding to the reverse. The value of H/B varies from 3 to 5, corresponding to four different values of $c_{u2}/\gamma B$, namely, 1, 2, 3, and 4. Following a previous study [7], three slope angles of β = 1:2, 1:1 and 2:1 are taken into consideration. The ranges of the parameters used in nondimensionalizing are γ = 20 kN·m^3 and B = 1 m, θ_x = 10 m and $c_{u1}/\gamma B$ = 2.

4.2.1 Effect of c_{u1}/c_{u2}

Figure 5 presents the effects of various undrained shear strength ratios c_{u1}/c_{u2} and coefficients of variation of cohesion of the upper layer soil COV_{cu1} on the mean ultimate bearing capacity factor μ_{Nc} and coefficients of variation of cohesion COV_{Nc}. The deterministic values of the bearing capacity factor for the three cases are shown as dashed lines in Fig. 5a (i.e., $N_{c,det}$ = 3.44). In general, the presence of spatial variability reduces the stability number

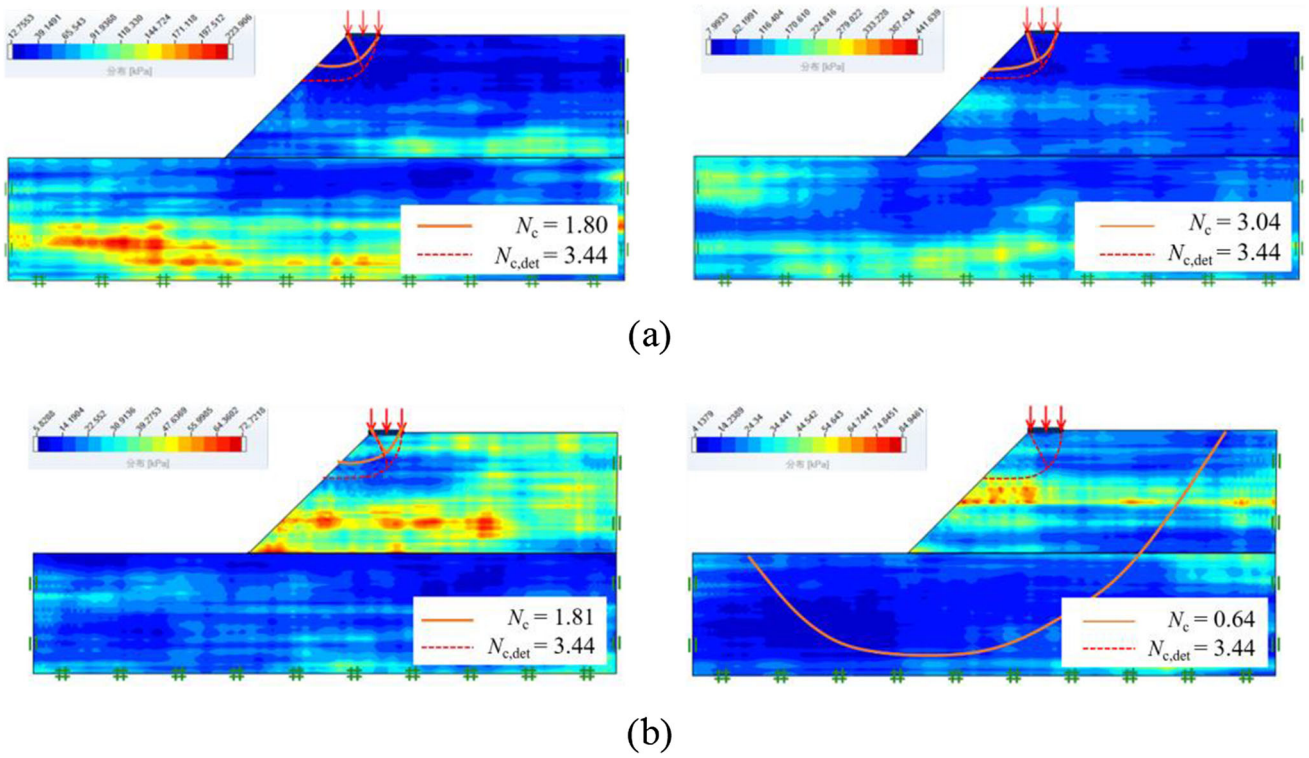

Fig. 8 Slip surfaces for different realizations of foundations with bearing capacity factors: **a** $c_{u1}/c_{u2} = 0.5$; **b** $c_{u1}/c_{u2} = 2$

compared to its deterministic value. In probabilistic analysis, any consideration of c_{u1}/c_{u2} yields a linearly decreased μ_{Nc} with an increasing COV_{cu1}, as shown in Fig. 5a. In contrast, an increasing COV_{Nc} for four curves (i.e., $c_{u1}/c_{u2} = 0.5$, 1, 1.5 and 2) is captured as COV_{cu1} increases. Specifically, the results of μ_{Nc} are similar when a small value (e.g., $c_{u1}/c_{u2} = 0.5$, 1 and 1.5), while a noticeable difference for the case with $c_{u1}/c_{u2} = 2$ is captured in comparison to these three cases. Similar to μ_{Nc}, the values of COV_{cu1} with $c_{u1}/c_{u2} = 0.5$, 1 and 1.5 exhibit an insignificant difference, while a larger COV_{cu1} is observed when $c_{u1}/c_{u2} = 2$, as presented in Fig. 5b.

The COV of the lower layer soil (i.e., COV_{cu2}) and c_{u1}/c_{u2} also influence the variability in N_c values. Figure 6a presents the relationships of μ_{Nc} with varied COV_{cu2} for different c_{u1}/c_{u2}, and the corresponding change in COV_{Nc} is shown in Fig. 6b. In comparison with the effect of COV_{cu1}, the values of μ_{Nc} and COV_{Nc} are insensitive to COV_{cu2} when $c_{u1}/c_{u2} = 0.5$, 1 and 1.5. For the case with $c_{u1}/c_{u2} = 2$, a monotonically reduced μ_{Nc} and an increased COV_{Nc} are attained as COV_{cu2} increases.

In conventional deterministic design, the failure can be defined as the bearing capacities of a footing being less than the corresponding deterministic values based on the uniform soil strength $N_{c,det}$ [8], and the value divided by a factor of safety (FS) is used to compute the allowable bearing pressure. Therefore, the value of P ($N_{c,i} < N_{c,det}$/FS) is of practical interest to describe the failure probability P_f. The change in the magnitude of P_f with the change in FS with various c_{u1}/c_{u2} for COV_{cu1} and COV_{cu2} is shown in Fig. 7. For FS = 1, the failure probability increases from 60 to 80% when c_{u1}/c_{u2} increases from 0.5 to 2, indicating a similar risk of failure. When FS = 2 and 3, a significant reduced factor is captured for c_{u1}/c_{u2} of 0.5, 1 and 1.5, and a larger FS is needed for c_{u1}/c_{u2} of 2. A relatively larger probability of failure for a larger c_{u1}/c_{u2} results from the relatively larger COV of the bearing capacity factor.

Prior investigations have shown that the soil strength has a paramount influence on the bearing capacity that can be attained on two-layered soil slopes, as it governs the failure mechanism that occurs [39, 41, 59]. In stochastic analysis, the spatial soil variability may result in variation of ultimate bearing capacities and potential failure mechanisms. To reveal the variation in the bearing capacity factor N_c when considering spatial soil variability, the failure mechanism of the footing on two-layered slopes is analyzed for various c_{u1}/c_{u2}. In probabilistic analysis, slip surfaces in random soil may develop several paths in weak soil instead of a single shear path [8, 9, 37]. The slip surfaces of various realizations are markedly different from one another because of the difference in the spatial patterns of random soil. In uniform soil, a failure slip extending to the slope face is observed (i.e., face failure mode) with N_c of 3.44 (see Fig. 4b), and an asymmetrical rigid wedge

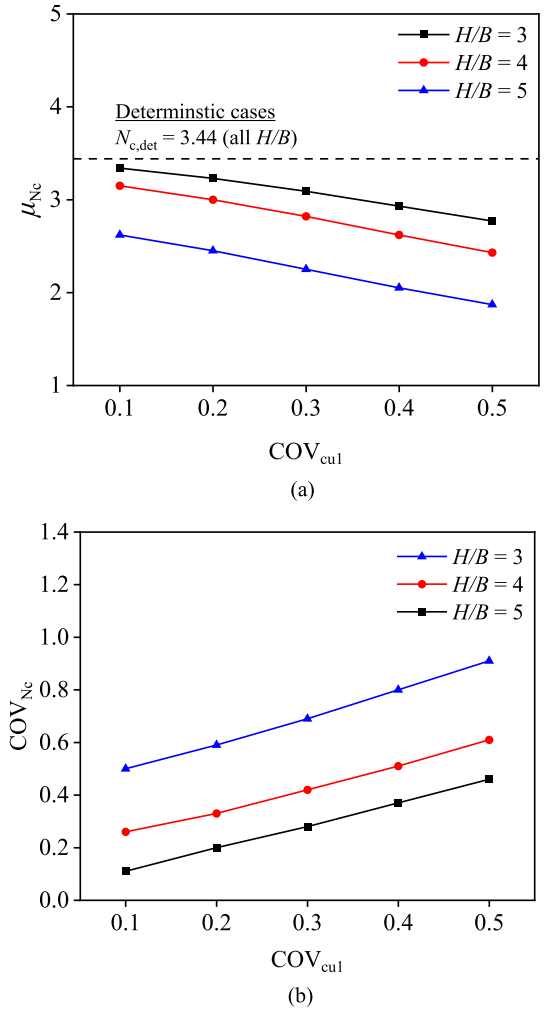

Fig. 9 Variation in μ_{Nc} and COV_{Nc} with COV_{cu1} for different normalized slope heights (H/B = 4 is the baseline case): **a** mean of N_c and **b** COV of N_c

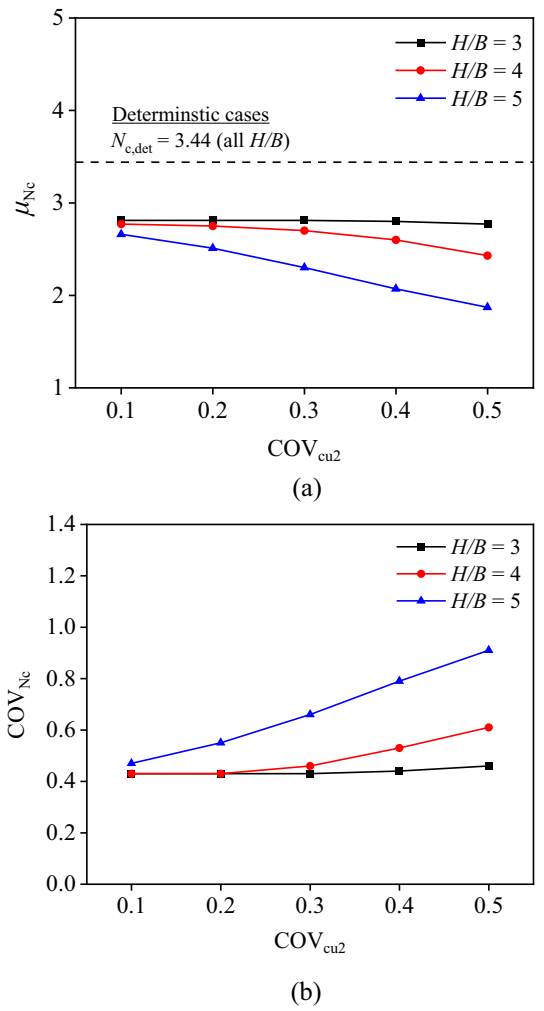

Fig. 10 Variation in μ_{Nc} and COV_{Nc} with COV_{cu2} for different normalized slope heights (H/B = 4 is the baseline case): **a** mean of N_c the **b** COV of N_c

occurs directly beneath the footing. In random soil, Fig. 8a and Fig. 8b selectively show the failure planes for footings with bearing capacity factors of 1.80 and 3.04 when c_{u1}/c_{u2} = 0.5, which both involve face failure. Failure mechanisms comparable to those in the deterministic case are captured. With reference to a comparable failure mechanism and slip surface length, the corresponding bearing capacity is reduced due to the soil strength along the slip surface. For c_{u1}/c_{u2} of 2, Fig. 8c also shows that face failure occurs with a bearing capacity factor of 1.81. Figure 8d illustrates that a shear surface extends far from the back corner of the footing (i.e., slope failure mode), which leads to a small resistance of the soil and thus a significantly reduced bearing capacity factor of 0.64. This is because the self-weight of the soil, acting as an external force, causes the failure of the slope rather than the contribution of the bearing capacity. Therefore, both the failure mechanism and the soil strength along the slip surface depend on the spatial pattern of the random field and determine the bearing capacity.

4.2.2 Effect of *H/B*

The effects of COV_{cu1} and the normalized slope height H/B on the mean bearing capacity μ_{Nc} and COV_{Nc} are presented in Fig. 9a, b, respectively. The deterministic results are also presented as a reference (i.e., $N_{c,\,det}$ = 3.44 for H/B = 3, 4 and 5).The three curves have a dip of μ_{Nc} with increasing COV_{cu1}, especially for the case with H/B = 5, as shown in Fig. 9a. For COV_{Nc}, a linear increase in COV_{Nc} with increasing COV_{cu1} is captured for any normalized slope height, as presented in Fig. 9b.

A parametric study for lower layer soil is also performed to evaluate COV_{cu2} = 0.1, 0.2, 0.3, 0.4 and 0.5 for H/B of 4, 5 and 6. The effect of COV_{cu2} and H/B on μ_{Nc} and COV_{Nc} is shown in Fig. 10. When H/B is large (i.e., $H/$

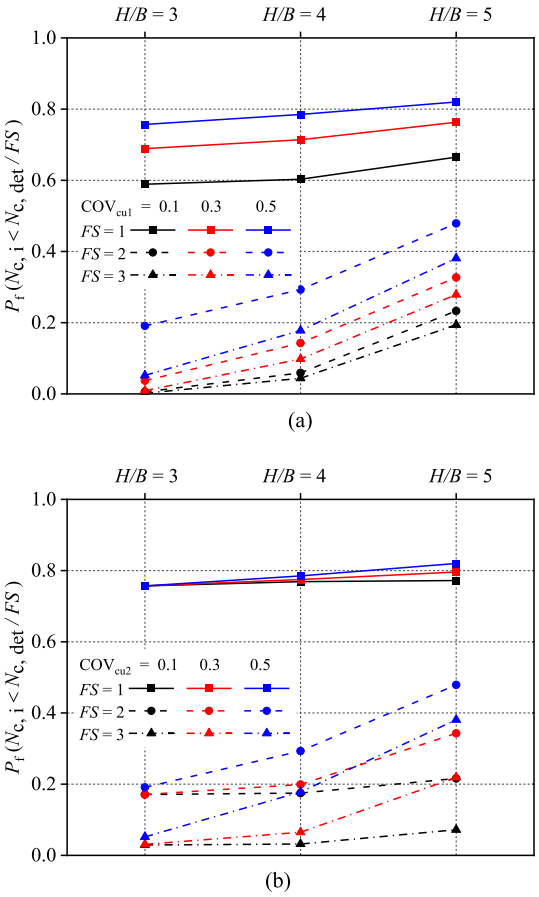

Fig. 11 Relationship between $P_f = P\ (N_{c,i} < N_{c,det}$ /FS) and H/B with various FS considering **a** COV_{cu1} and **b** COV_{cu2}

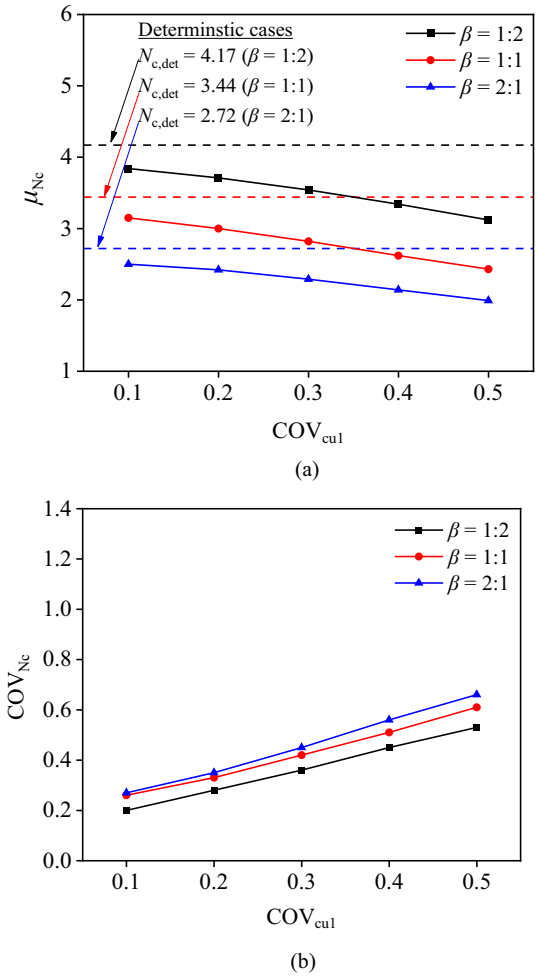

Fig. 12 Variation of μ_{Nc} and COV_{Nc} with COV of COV_{cu2} for different slope gradients, β (β = 1:1 is the baseline case): **a** mean of N_c **b** COV of N_c

B = 6), the largest influence of lower layer soil variability is observed. Larger H/B values correspond to the largest relative decreases in $\mu_{Nc,}$ and then the increases in COV_{Nc} are also most pronounced. In contrast, a smaller H/B causes μ_{Nc} and COV_{Nc} to be less sensitive to changes in COV_{cu2}. The relationship of P_f of various H/B with FS = 1, 2 and 3 is shown in Fig. 11. It is interesting to see that for H/B = 4, 5 and 6 with different COV_{cu1} and COV_{cu2} give similar probability of design failure when FS = 1. For FS = 2 and 3, the results demonstrate that a footing with a large H/B has a larger probability of failure.

4.2.3 Effect of β

Figure 12a shows the change in μ_{Nc} and COV_{Nc} with COV_{cu1} for various slope angles β. The deterministic results are also presented as a reference (i.e., $N_{c,\ det}$ = 2.72, 3.44 and 4.17 for β = 2:1, 1:1 and 1:2). As expected, consideration of larger values of COV_{cu1} resulted in increased μ_{Nc}. The largest proportional decrease in μ_{Nc} occurs for steeper slopes. As shown in Fig. 12b, a trend of linear increase in COV_{Nc} is represented for all slope angles in this study. However, a larger slope angle is less sensitive to changes in COV_{cu1}.

To investigate the influence of COV_{cu2} and slope angle β, the change in μ_{Nc} and COV_{Nc} for β = 1:2, 1:1 and 2:1 with various COV_{cu2} is shown in Fig. 13. Similar to the effect of the upper layer soil variability, a monotonous decrease in μ_{Nc} and an increase in COV_{Nc} are also caused by increasing COV_{cu2} under any consideration of β. Notably, the influence of COV_{cu2} on μ_{Nc} is more significant for a small slope angle (e.g., β = 1:2), and a large slope angle causes slope μ_{Nc} to be less sensitive to changes in COV_{cu2}. The divergence of COV_{Nc} for these three curves is not pronounced, showing a lower sensitivity to β with different COV_{cu2}. The relationship of P_f of various β with FS = 1, 2 and 3 is presented in Fig. 14. With different β, a similar probability of design failure is captured when the values of FS are the same. For FS = 1, the failure probability increases from 55 to 80% when COV_{cu1} increases from 0.5 to 2, indicating a similar risk of failure. In

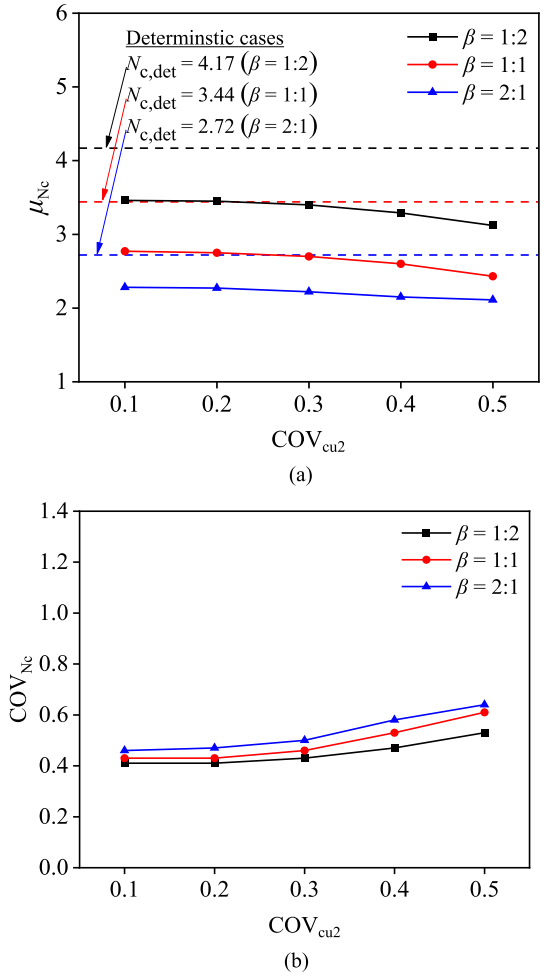

Fig. 13 Variation in μ_{Nc} and COV_{Nc} with COV_{cu2} for different slope gradients, β (β = 1:1 is the baseline case): **a** mean of N_c the **b** COV of N_c

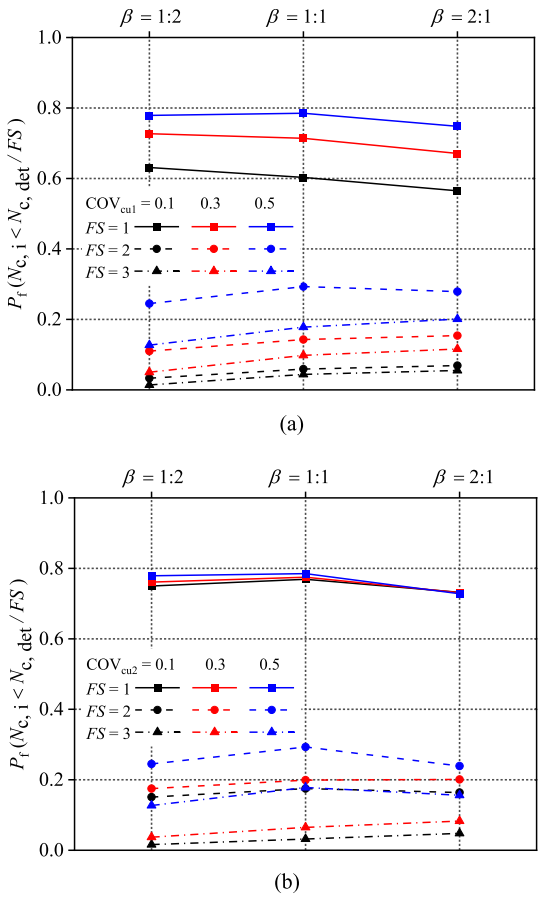

Fig. 14 Relationship between $P_f = P$ ($N_{c,i} < N_{c,det}$/FS) and β with various FS considering **a** COV_{cu1} and **b** COV_{cu2}

contrast, the effect of COV_{cu2} could be neglected. When FS = 2 and 3, a significant reduced P_f is captured for various COV_{cu1} and COV_{cu2}.

5 Discussion

The aforementioned analyses reveal that the coupling effects of the soil spatial correlation parameters (COV_{cu1}, COV_{cu2}, θ_y/θ_x), soil properties (c_{u1}/c_{u2}) and geometric parameters (H/B and β) on the ultimate bearing capacity are distinct and complex. Investigations of the sensitivity of each parameter on the mean μ_{Nc} and coefficient of variation of the bearing capacity factor COV_{Nc} are of great importance because they provide practical guidance for the footing placed on a two-layered slope when considering spatial soil variability.

5.1 Sensitivity analysis

In this study, a sensitivity analysis using multivariate adaptive regression splines (MARS) [5, 35, 38, 50, 54] is conducted to quantify the effects of soil properties and geometrical parameters on the bearing capacity factor considering spatial soil variability. MARS is an algorithm for mathematically describing the relationship between a set of input and output variables, which has thus been successfully applied in various geotechnical engineering applications [47–49, 52]. Without undertaking a training process or specific assumptions, a simple model can be produced by a MARS model that can be easily interpreted and analyze the relative importance of each parameter. The end points of the segments (splines), which are called knots or nodes, mark the end of one piecewise set of data and the beginning of another. The resulting piecewise curves, known as basis functions (BFs), allow for bending, thresholds and other nonlinear feature. The data partition of this study is conducted through random approach, 75% of the data were used for training and 25% for testing, the subsets for training and testing are statistically consistent

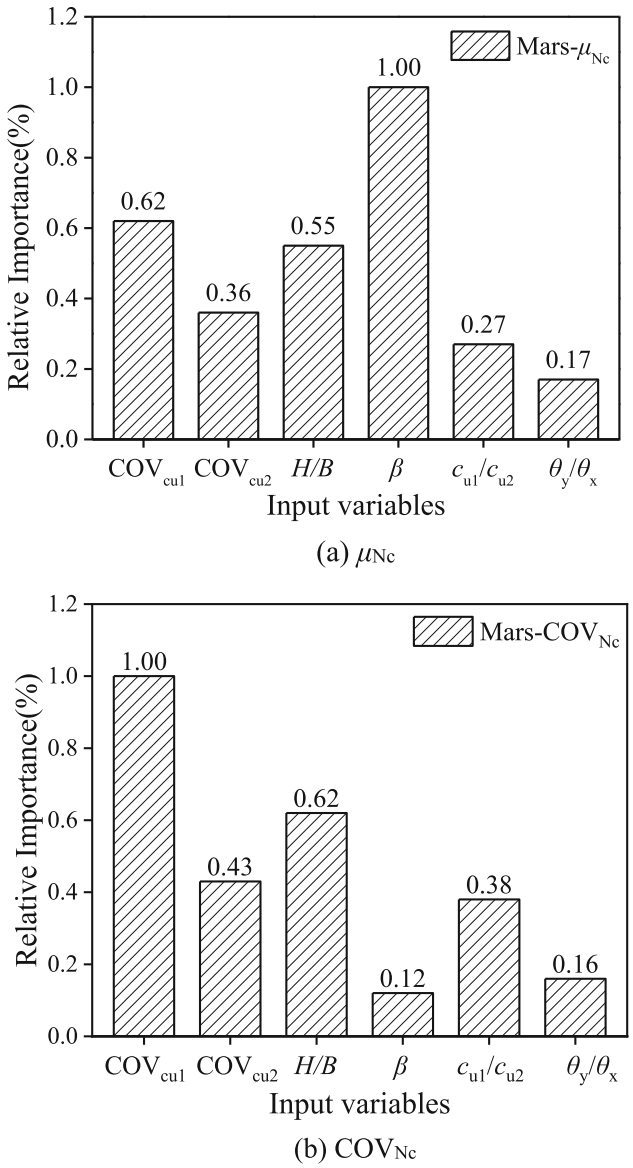

Fig. 15 Importance index of each variable: **a** μ_{Nc}; **b** COV_{Nc}

Table 3 ANOVA decomposition of the MARS model of μ_{Nc}

Number	Variable(s)	*GCV*	R^2_{GCV}
1	COV_{cu2}, *H/B*	0.00625	0.96307
2	COV_{cu2}, c_{u1}/c_{u2}	0.00437	0.97416
3	COV_{cu2}, *H/B*, c_{u1}/c_{u2}	0.00155	0.99082
4	COV_{cu2}, c_{u1}/c_{u2}, θ_y/θ_x	0.00149	0.9912
5	COV_{cu1}, β	0.00142	0.99161
6	COV_{cu1}, COV_{cu2}, c_{u1}/c_{u2}	0.0013	0.99229
7	COV_{cu1}, COV_{cu2}, *H/B*, c_{u1}/c_{u2}	0.001	0.9941

and therefore represent the population. This algorithm can mathematically identify optimal variable transformations and complex interactions between the output and high-dimensional input variables, which could be employed in this study to illustrate the complex response between the bearing capacity and spatial clays.

Table 4 ANOVA decomposition of the MARS model of COV_{Nc}

Number	Variable(s)	*GCV*	R^2_{GCV}
1	COV_{cu2}, c_{u1}/c_{u2}	0.00223	0.93669
2	COV_{cu2}, *H/B*	0.00091	0.9743
3	COV_{cu2}, *H/B*, c_{u1}/c_u, θ_y/θ_x	0.00073	0.9794
4	COV_{cu2}, c_{u1}/c_{u2}, θ_y/θ_x	0.00032	0.99079
5	COV_{cu2}, β, c_{u1}/c_{u2}	0.00028	0.99217
6	β, c_{u1}/c_{u2}	0.00026	0.99257
7	COV_{cu1}, COV_{cu2}, *H/B*, c_{u1}/c_{u2}	0.00025	0.9929
8	COV_{cu1}, COV_{cu2}, β, c_{u1}/c_{u2}	0.00024	0.99312
9	COV_{cu2}, θ_y/θ_x	0.00022	0.99386

Six affecting parameters x_1 (COV_{cu1}), x_2 (COV_{cu2}), x_3 (*H/B*), x_4 (β), x_5 (c_{u1}/c_{u2}) and x_6 (θ_y/θ_x), as mentioned above, are selected as input variables, and the output variables are the mean and coefficient of variation of the bearing capacity (μ_{Nc} and COV_{Nc}). Figure 15 shows the relative importance of each input variable estimated by adopting the MARS procedure. The relative importance describes the contribution and the degree of sensitivity of each input variable to μ_{Nc} and COV_{Nc} [47]. Notably, x_4 (β) and x_1 (COV_{cu1}) are the most important variables for the values of y_1 (μ_{Nc}) and y_2 (COV_{Nc}), respectively, in which the index of relative importance (IRI) is equal to 1.0. Correspondingly, the following variables for y_1 (μ_{Nc}) are x_1 (COV_{cu1}), x_3 (*H/B*), x_2 (COV_{cu2}), x_5 (c_{u1}/c_{u2}) and x_6 (θ_y/θ_x), with IRIs of 0.63, 0.55, 0.36, 0.27 and 0.15, respectively. For the coefficient of variation of the bearing capacity COV_{Nc}, the descending order is presented with reference to the importance of contributions as follows: x_3 (*H/B*), x_2 (COV_{cu2}), x_5 (c_{u1}/c_{u2}), x_6 (θ_y/θ_x) and x_4 (β) with IRIs of 0.61, 0.46, 0.40, 0.17 and 0.14, respectively. The results indicate that a noticeable effect of the slope angle β is presented on μ_{Nc}, and COV_{cu1} also has an apparent influence on COV_{Nc}.

5.2 Coupled effects

To present the coupled influence of the soil properties and geometrical parameters while considering spatial soil variability, a variance decomposition procedure (ANOVA) is applied [46, 47]. Tables 3 and 4 summarize the ANOVA functions of the proposed MARS model, reflecting the interaction effects of those input variables. A large, generalized cross-validation (GCV) value or a relatively small R^2_{GCV} value indicates a significant ability of their

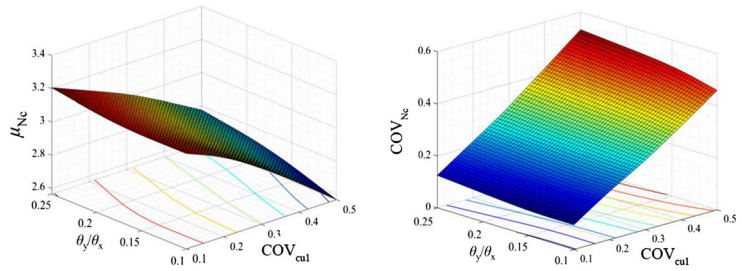
μ_{Nc}
θ_y/θ_x
COV_{cu1}
COV_{Nc}

(a)

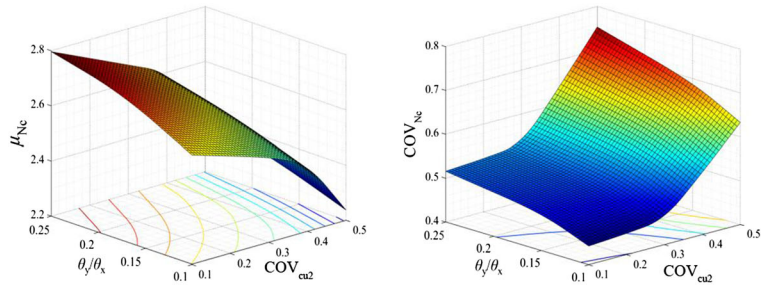
μ_{Nc}
θ_y/θ_x
COV_{cu2}
COV_{Nc}

(b)

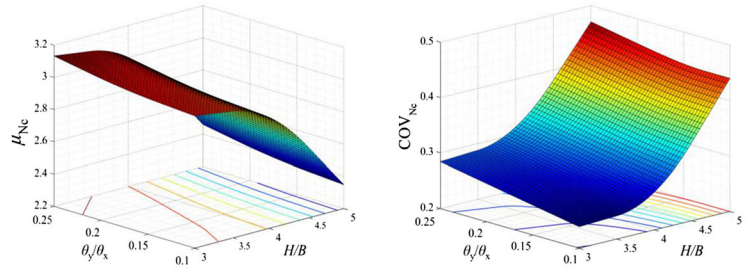
μ_{Nc}
θ_y/θ_x
H/B
COV_{Nc}

(c)

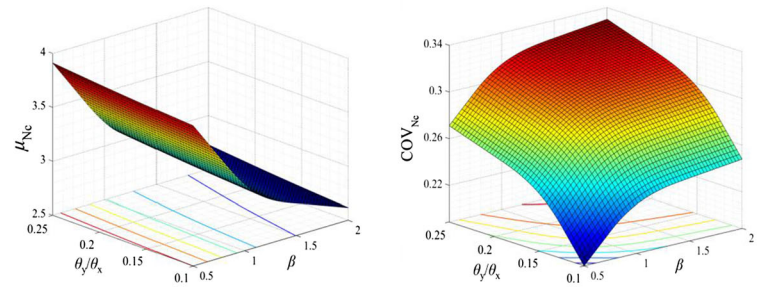
μ_{Nc}
θ_y/θ_x
β
COV_{Nc}

(d)

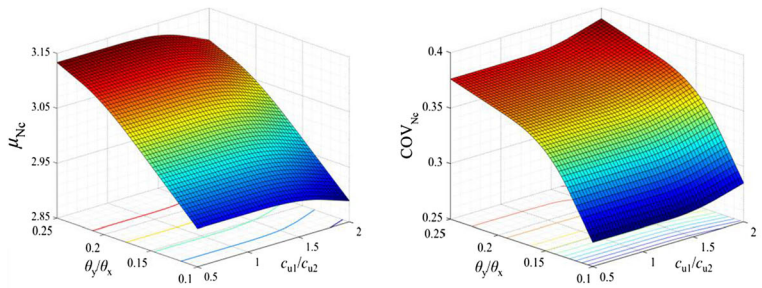
μ_{Nc}
θ_y/θ_x
c_{u1}/c_{u2}
COV_{Nc}

(e)

◀**Fig. 16** Variation of μ_{Nc} and COV_{Nc} with the affecting factors for different anisotropic spatial correlation length ratios θ_y/θ_x: **a** COV_{cu1}; **b** COV_{cu2}; **c** normalized slope height H/B; **d** slope angle β; **e** undrained shear strength ratio c_{u1}/c_{u2}

interactions to affect the output value (i.e., μ_{Nc} and COV_{Nc}). As shown in Table 3, the most pronounced interaction effect on μ_{Nc} is captured between the input variables of COV_{cu2} and H/B. In addition, the COV_{cu2} coupled effect between COV_{Nc} and other determinate input variables (e.g., c_{u1}/c_{u2} and β) is also emphasized with reference to the GCV value. For COV_{Nc}, the most important interaction is between COV_{cu2} and c_{u1}/c_{u2}. Similar to μ_{Nc}, COV_{cu2}, coupled with other determinate geometric variables (e.g., H/B and β), has a noticeable effect on COV_{Nc}. The coupled effect of COV_{cu2} summarized in Tables 3 and 4 coincides with the results of parametric analysis in Sect. 4.2.

As shown in Tables 3 and 4, in addition to COV_{cu2}, the values of μ_{Nc} and COV_{Nc} are also sensitive to the coupled effect between the anisotropic spatial correlation length ratio θ_y/θ_x and other variables. Figure 16 plots the coupled effects between x_6 (θ_y/θ_x) and five parameters (i.e., x_1 (COV_{cu1}), x_2 (COV_{cu2}), x_3 (H/B), x_4 (β) and x_5 (c_{u1}/c_{u2})) on the values of y_1 (μ_{Nc}) and y_2 (COV_{Nc}). As shown in Fig. 16a, b, it can be concluded from the contour lines that the roles of COV_{cu1} and COV_{cu2} in governing the values of μ_{Nc} and COV_{Nc} become increasingly important in comparison with that of θ_y/θ_x. Specifically, COV_{Nc} and μ_{Nc} are less sensitive to θ_y/θ_x for different COV_{cu1}. However, both the values of μ_{Nc} and COV_{Nc} have a greater sensitivity to θ_y/θ_x for a large COV_{cu2} due to the coupled effect between COV_{cu2} and COV_{Nc}. When θ_y/θ_x is coupled with soil properties and geometric parameters, the interaction effects between those variables are shown in Fig. 16c–e. Specifically, for H/B and β, the coupled effect with θ_y/θ_x induces the highest COV_{Nc}, while that of large COV_{cu2} and small θ_y/θ_x is captured with a large value of μ_{Nc}. When coupled with c_{u1}/c_{u2}, θ_y/θ_x noticeably contributes to limiting the values of μ_{Nc} and COV_{Nc} in comparison with that of c_{u1}/c_{u2}.

6 Conclusion

In this paper, a RAFELA method is adopted to investigate the effect of soil spatial variability on the ultimate bearing capacity and associated failure mechanisms. The properties of soils are defined by random field theory. The stochastic analysis is carried out using the Monte Carlo simulation technique. On this basis, comprehensive studies on cases with different undrained shear strength ratios, normalized slope heights and slope angles are conducted, offering deeper insight into how the bearing capacity quantitatively changes and couples with variations in slope geometry, soil properties and soil spatial variability. Moreover, the sensitivity of the parameters is discussed through a MARS model. The following conclusions can be drawn:

1. The spatial variability of the soil parameter is taken into consideration for different coefficients of variation (COVs) of two-layered soils. With reference to two-layered soil variability, the soil properties and geometric conditions all affect the variability of the ultimate bearing capacity of rigid footings on two-layered soil slopes. Increasing c_{u1}/c_{u2}, H/B, and β leads to a smaller mean and larger coefficient of variation of the bearing capacity when affecting factors are considered.
2. Soil properties (c_{u1}/c_{u2}) and geometric parameters (e.g., H/B and β) are found to have coupled effects with soil variability (e.g., θ_y/θ_x, COV_{cu1} and COV_{cu2}) on the mean and coefficient of variation of bearing capacity (μ_{Nc} and COV_{Nc}). One notable effect is tied to an increase in the variability of lower layer soils (COV_{cu2}), in which increasing COV_{cu2} with different H/B, β and c_{u1}/c_{u2}, respectively, leads to a rapid change in μ_{Nc} and COV_{Nc}.
3. A nonlinear relationship between a set of input variables (i.e., COV_{cu1}, COV_{cu2}, H/B, β, c_{u1}/c_{u2}) and output variables (i.e., μ_{Nc} and COV_{Nc}) is captured. The artificial data for the sensitivity analysis are generated through limit analysis considering spatial soil variability. According to the MARS procedure, the slope angle β is the most important variable for the values of μ_{Nc}, followed by the parameters of COV_{cu1}, H/B, COV_{cu2}, c_{u1}/c_{u2} and θ_y/θ_x. For the effect of these input variables on COV_{Nc}, COV_{cu1}, as the most important variable, is followed by H/B, COV_{cu2}, c_{u1}/c_{u2}, θ_y/θ_x and β.
4. Design guidance for engineering practice is provided for different anisotropic spatial correlation length ratios θ_y/θ_x. Significant COV_{cu2} H/B and β values are required for ensuring the bearing capacity factors owing to noticeable interaction effects with θ_y/θ_x. Furthermore, the coupled effect of θ_y/θ_x with the COV of upper layered clay COV_{cu1} and undrained shear strength ratio c_{u1}/c_{u2} can be neglected on μ_{Nc} and COV_{Nc}.

The limitation of the work in this paper is that the c–φ soil slope has not been involved. Investigating the influence of various thicknesses of the two layers of soils on the bearing capacity is also beyond the scope of this investigation. They are expected to be discussed in future work. In addition, upper-bound solutions are selected to investigate the influence of the footing distance on the bearing capacity. The investigation is focused on the understanding

of the effect of affecting factors rather than an exact quantitative solution.

Acknowledgements This research was funded by the National Natural Science Foundation of China (No. 52208363), the China National Postdoctoral Program for Innovative Talents (No. BX20220225), the Project of Tianjin Science and Technology Plan (No. 22JCQNJC01140), the China Postdoctoral Science Foundation (No. 2022M722371), the National Natural Science Foundation of China (No. 52078337), the Project of Tianjin Science and Technology Plan (No. 21JCZXJC00070).

Data availability All data generated or analyzed during this study are included in this published article.

Declarations

Conflict of interest The authors declare that they have no known competing financial interests or personal relationships that could have appeared to influence the work reported in this paper.

References

1. Azzouz AS, Baligh MM (1983) Loaded areas on cohesive slopes. J Geotech Eng 109(5):724–729
2. Ali A, Lyamin AV, Huang J, Li JH, Cassidy MJ, Sloan SW (2017) Probabilistic stability assessment using adaptive limit analysis and random fields. Acta Geotech 12(4):937–948
3. Choudhuri K, Chakraborty D (2021) Probabilistic bearing capacity of a pavement resting on fibre reinforced embankment considering soil spatial variability. Front Built Environ 7:628016
4. Choudhuri K, Chakraborty D (2022) Probabilistic analyses of three-dimensional circular footing resting on two-layer c–φ soil system considering soil spatial variability. Acta Geotech 17(12):5739–5758
5. Friedman JH (1991) Multivariate adaptive regression spline. Ann Stat 19(1):1–67
6. Foroutan Kalourazi A, Jamshidi Chenari R, Veiskarami M (2020) Bearing capacity of strip footings adjacent to anisotropic slopes using the lower bound finite element method. Int J Geomech 20(11):04020213
7. Georgiadis K (2010) Undrained bearing capacity of strip footings on slopes. J Geotech Geoenviron Eng 136(5):677–685
8. Griffiths DV, Fenton GA (2001) Bearing capacity of spatially random soil: the undrained clay Prandtl problem revisited. Geotechnique 51(4):351–359
9. Griffiths DV, Fenton GA, Manoharan N (2002) Bearing capacity of rough rigid strip footing on cohesive soil: probabilistic study. J Geotech Geoenviron Eng 128(9):743–755
10. Guo S, Griffiths DV (2020) Failure mechanisms in two-layer undrained slopes. Can Geotech J 57(10):1617–1621
11. Halder K, Chakraborty D (2019) Probabilistic bearing capacity of strip footing on reinforced soil slope. Comput Geotech 116:103213
12. Halder K, Chakraborty D (2020) Influence of soil spatial variability on the response of strip footing on geocell-reinforced slope. Comput Geotech 122:103533
13. Hu P, Stanier SA, Cassidy MJ, Wang D (2014) Predicting peak resistance of spudcan penetrating sand overlying clay. J Geotech Geoenviron Eng 140(2):04013009
14. Izadi A, Foroutan Kalourazi A, Jamshidi Chenari R (2021) Effect of roughness on seismic bearing capacity of shallow foundations near slopes using the lower bound finite element method. Int J Geomech 21(3):06020043
15. Kalourazi AF, Izadi A, Chenari RJ (2019) Seismic bearing capacity of shallow strip foundations in the vicinity of slopes using the lower bound finite element method. Soils Found 59(6):1891–1905
16. Keawsawasvong S, Ukritchon B (2019) Undrained basal stability of braced circular excavations in non-homogeneous clays with linear increase of strength with depth. Comput Geotech 115:103180
17. Keawsawasvong S, Ukritchon B (2019) Undrained stability of a spherical cavity in cohesive soils using finite element limit analysis. J Rock Mech Geotech Eng 11(6):1274–1285
18. Krabbenhoft K, Lymain AV, Krabbenhoft J (2016) OptumG2: theory. Newcastle, Australia: Optum Computational Engineering
19. Kusakabe O, Kimura T, Yamaguchi H (1981) Bearing capacity of slopes under strip loads on the top surfaces. Soils Found 21(4):29–40
20. Leshchinsky B, Ambauen S (2015) Limit equilibrium and limit analysis: comparison of benchmark slope stability problems. J Geotech Geoenviron Eng 141(10):04015043
21. Leshchinsky B (2015) Bearing capacity of footings placed adjacent to e'–ϕ' slopes. J Geotech Geoenviron Eng 141(6):04015022
22. Li X, Pei X, Gutierrez M, He S (2012) Optimal location of piles in slope stabilization by limit analysis. Acta Geotech 7(3):253–259
23. Li XY, Zhang LM, Gao L, Zhu H (2017) Simplified slope reliability analysis considering spatial soil variability. Eng Geol 216:90–97
24. Li K, Li D, Liu Y (2020) Meso-scale investigations on the effective thermal conductivity of multi-phase materials using the finite element method. Int J Heat Mass Tran 151:119383. https://doi.org/10.1016/j.ijheatmasstransfer.2020.119383
25. Li K, Miao Z, Li D, Liu Y (2022) Effect of mesoscale internal structure on effective thermal conductivity of anisotropic geomaterials. Acta Geotech 17(8):3553–3566
26. Li K, Kang Q, Nie J, Huang X (2022) Artificial neural network for predicting the thermal conductivity of soils based on a systematic database. Geothermics 103:102416. https://doi.org/10.1016/j.geothermics.2022.102416
27. Luo N, Bathurst RJ (2017) Reliability bearing capacity analysis of footings on cohesive soil slopes using RFEM. Comput Geotech 89:203–212
28. Meyerhof GG (1957) The ultimate bearing capacity of foundations on slopes. In: Proceedings of the international conference on soil mechanics and foundation engineering, vol 1, pp 384–386
29. Meyerhof GG (1974) Ultimate bearing capacity of footings on sand layer overlying clay. Can Geotech J 11(2):223–229
30. Merifield RS, Sloan SW, Yu HS (1999) Rigorous plasticity solutions for the bearing capacity of two-layered clays. Geotechnique 49(4):471–490
31. Phoon KK, Kulhawy FH (2005) Characterization of model uncertainties for laterally loaded rigid drilled shafts. Geotechnique 55(1):45–54
32. Phoon KK (2008) Reliability-based design in geotechnical engineering: computations and applications. CRC Press, Boca Raton
33. Phoon KK, Ching J (2015) Risk and reliability in geotechnical engineering. CRC Press, Boca Raton
34. Qin C, Zhou J (2023) On the seismic stability of soil slopes containing dual weak layers: true failure load assessment by finite-element limit-analysis. Acta Geotech. In press. https://doi.org/10.1007/s11440-022-01730-2
35. Rudy J (2016) py-earth: a Python implementation of Jerome Friedman's multivariate adaptive regression splines. https://github.com/jcrudy/py-earth. Accessed 18 Aug 2021

36. Sloan SW, Kleeman PW (1995) Upper bound limit analysis using discontinuous velocity fields. Comput Methods Appl Mech Eng 127(1–4):293–314
37. Tang C, Phoon KK, Zhang L, Li DQ (2017) Model uncertainty for predicting the bearing capacity of sand overlying clay. Int J Geomech 17(7):04017015
38. Wang L, Wu C, Gu X, Liu H, Mei G, Zhang W (2020) Probabilistic stability analysis of earth dam slope under transient seepage using multivariate adaptive regression splines. Bull Eng Geol Environ 79(6):2763–2775
39. Wu G, Zhao H, Zhao M, Xiao Y (2020) Undrained seismic bearing capacity of strip footings lying on two-layered slopes. Comput Geotech 122:103539
40. Wu G, Zhao H, Zhao M, Duan L (2023) Ultimate bearing capacity of strip footings lying on Hoek–Brown slopes subjected to eccentric load. Acta Geotech 18(2):1111–1124
41. Xiao Y, Zhao M, Zhang R, Zhao H, Wu G (2019) Undrained bearing capacity of strip footings placed adjacent to two-layered slopes. Int J Geomech 19(8):06019014
42. Xie Y, Leshchinsky B, Han J (2019) Evaluation of bearing capacity on geosynthetic-reinforced soil structures considering multiple failure mechanisms. J Geotech Geoenviron Eng 145(9):04019040
43. Yang S, Leshchinsky B, Cui K, Zhang F, Gao Y (2019) Unified approach toward evaluating bearing capacity of shallow foundations near slopes. J Geotech Geoenviron Eng 145(12):04019110
44. Yang S, Leshchinsky B, Cui K, Zhang F, Gao Y (2021) Influence of failure mechanism on seismic bearing capacity factors for shallow foundations near slopes. Géotechnique 71(7):594–607
45. Yodsomjai W, Keawsawasvong S, Lai VQ (2021) Limit analysis solutions for bearing capacity of ring foundations on rocks using Hoek-Brown failure criterion. Int J Geosynthet Gr Eng 7(2):1–10
46. Zhang W, Goh ATC, Xuan F (2015) A simple prediction model for wall deflection caused by braced excavation in clays. Comput Geotech 63:67–72
47. Zhang W, Goh ATC (2016) Evaluating seismic liquefaction potential using multivariate adaptive regression splines and logistic regression. Geomech Eng 10(3):269–284
48. Zhang W, Zhang Y, Goh ATC (2017) Multivariate adaptive regression splines for inverse analysis of soil and wall properties in braced excavation. Tunnel Undergr Space Technol 64:24–33
49. Zheng G, He X, Zhou H, Yang X, Yu X, Zhao J (2020) Prediction of the tunnel displacement induced by laterally adjacent excavations using multivariate adaptive regression splines. Acta Geotech 15:2227–2237
50. Zheng G, Zhang W, Zhou H, Yang P (2020) Multivariate adaptive regression splines model for prediction of the liquefaction-induced settlement of shallow foundations. Soil Dyn Earthq Eng 132:106097
51. Zheng G, Zhao J, Zhou H (2021) Ultimate bearing capacity of two interfering strip footings on sand overlying clay. Acta Geotech 16(7):2301–2311
52. Zhou H, Diao Y, Zheng G, Han J, Jia R (2017) Failure modes and bearing capacity of strip footings on soft ground reinforced by floating stone columns. Acta Geotech 12(5):1089–1103
53. Zheng G, He X, Zhou H (2023) A Prediction Model for the Deformation of an Embedded Cantilever Retaining Wall in Sand. Int J Geomech 23(3):06023001
54. Zhou H, Xu H, Yu X, Guo Z, Zheng G, Yang X, Tian Y (2021) Evaluation of the bending failure of columns under an embankment loading. Int J Geomech 21(7):04021112
55. Zhou H, Zheng G, Yin X, Jia R, Yang X (2018) The bearing capacity and failure mechanism of a vertically loaded strip footing placed on the top of slopes. Comput Geotech 94:12–21
56. Zhou H, Zheng G, Yang X, Li T, Yang P (2019) Ultimate seismic bearing capacities and failure mechanisms for strip footings placed adjacent to slopes. Can Geotech J 56(11):1729–1735
57. Zhou H, Shi Y, Yu X, Xu H, Zheng G, Yang S, He Y (2023) Failure mechanism and bearing capacity of rigid footings placed on top of cohesive soil slopes in spatially random soil. Int J Geomech. In press. https://doi.org/10.1061/IJGNAI/GMENG-8306
58. Zhang J, Phoon K, Zhang D, Huang H, Tang C (2021) Novel approach to estimate vertical scale of fluctuation based on CPT data using convolutional neural networks. Eng Geol 294:106342. https://doi.org/10.1016/j.enggeo.2021.106342
59. Zhou J, Qin C (2022) Stability analysis of unsaturated soil slopes under reservoir drawdown and rainfall conditions: Steady and transient state analysis. Comput Geotech 142:104541. https://doi.org/10.1016/j.compgeo.2021.104541